AIAA JOURNAL
Vol. 40, No. 12, December 2002

Relationship Between Upstream Turbulent Boundary-Layer Velocity Fluctuations and Separation Shock Unsteadiness

S. J. Beresh,* N. T. Clemens,† and D. S. Dolling‡
University of Texas at Austin, Austin, Texas 78712-1085

Particle image velocimetry and high-frequency response wall pressure measurements have been used to investigate the relationship between upstream turbulent boundary-layer properties and the unsteady separation shock behavior in a Mach 5 unswept compression ramp interaction. No correlation is found between variations in the incoming boundary-layer thickness and the separation shock foot position, as has been suggested in earlier work. However, the mean velocity profile, conditioned on the separation shock foot position, exhibits a subtly fuller shape when the shock is downstream than when it is upstream. More significantly, a clear correlation is observed between positive streamwise velocity fluctuations in the lower third of the upstream boundary layer and downstream shock motions, and vice versa. The strongest correlations are found for velocity fluctuations with frequencies of about 4–10 kHz, which is significantly lower than the frequencies that characterize the large-scale structures in the boundary layer (40 kHz), although spatial limitations in the transducer array may limit the instrument sensitivity to this lower range. These results are qualitatively consistent with the simple physical principle that a fuller velocity profile imparts increased resistance to separation to the boundary layer and, hence, causes downstream shock motion, whereas a less-full velocity profile is associated with lower resistance to separation and, hence, upstream shock motion.

Nomenclature

M = Mach number
P = pressure
T = temperature
U = mean streamwise velocity
u = local streamwise velocity
u' = local streamwise velocity fluctuation
γ = separation shock foot intermittency
δ_0 = boundary-layer thickness, 0.99 U_∞

Subscripts

0 = stagnation condition
∞ = freestream condition

I. Introduction

WORK in a broad range of supersonic separated turbulent flows has shown that separation is unsteady and that the separation shock foot motion and the expansion/contraction (or pulsation) of the separated flow can be described as a low-frequency, large-scale motion superimposed on which is a high-frequency, small-scale motion.[1–13] An example of the separation shock foot position history deduced from simultaneous, multichannel wall pressure signals in a separated unswept compression ramp flow at Mach 5 is shown in Fig. 1. The time history clearly exhibits a broad range of motions and frequencies.

Erengil and Dolling's[12] experimental studies of separation shock foot unsteadiness showed a correlation between the wall pressure fluctuations beneath the incoming boundary layer and the shock foot velocity, from which it was inferred that the small-scale motion of the shock is caused by its response to the convection of turbulent fluctuations through the interaction. It also was shown in Ref. 12 that the large-scale motion is a result of the shock's displacement due to the expansion and contraction of the separation bubble, similar to that observed by Kussoy et al.[2] A physical model of the shock unsteadiness was developed from these observations, in which the expansion and contraction of the separation bubble displaces the shock upstream or downstream, whereas the passage of turbulent fluctuations alters the shock velocity, which integrates to changes in the shock position and accounts for the small-scale high-frequency unsteadiness. Although this model offers an explanation for the small-scale motion, it does not address the cause of the low-frequency, large-scale pulsation of the separated flow.

McClure[9] and Ünalmis and Dolling[14] showed that the mean pitot pressure at a fixed vertical position in the upstream boundary layer was lower for upstream separation shock foot locations than for downstream locations, suggesting that low-frequency variations in the incoming boundary-layer thickness might induce the large-scale shock motion. Chan[15] and Beresh et al.[16,17] examined this idea using planar laser imaging techniques simultaneously with fluctuating wall pressure measurements, but found no significant correlation between the upstream boundary-layer thickness and the shock foot location. However, some exploratory particle image velocimetry (PIV) measurements of Beresh et al.[16] did indicate a small difference in velocity profile shape correlated to upstream and downstream shock foot locations. Overall, these findings provided little support for the thickening/thinning boundary-layer mechanism. Note, however, that Ünalmis and Dolling[14] found a difference of only about 5% in the pitot pressure between shock-upstream and shock-downstream conditions, which would correspond to a difference of less than 1% (about 5 m/s) in velocity. It is possible, then, that the thickening/thinning mechanism was not detectable within the precision of those previous measurements.

Beresh et al.[17] visualized a Mach 5 compression ramp interaction by using double-pulse planar laser scattering (PLS) from a seeded alcohol fog. Although the image pairs showed that the passage of individual large-scale turbulent structures distorted the outer region of the separation shock, the shock foot did not move appreciably in the time it took for the structures to convect through the shock. This suggests that large-scale boundary-layer structures may not significantly influence the shock foot behavior. Also in Ref. 17,

Received 5 September 2001; revision received 14 August 2002; accepted for publication 15 August 2002.

*Graduate Student, Department of Aerospace Engineering and Engineering Mechanics, Center for Aeromechanics Research; currently Senior Member of the Technical Staff, Engineering Sciences Center, Sandia National Laboratories, P.O. Box 5800, Mailstop 0834, Albuquerque, NM 87185.

†Associate Professor, Department of Aerospace Engineering and Engineering Mechanics, Center for Aeromechanics Research. Senior Member AIAA.

‡Professor, Department of Aerospace Engineering and Engineering Mechanics, Center for Aeromechanics Research. Fellow AIAA.

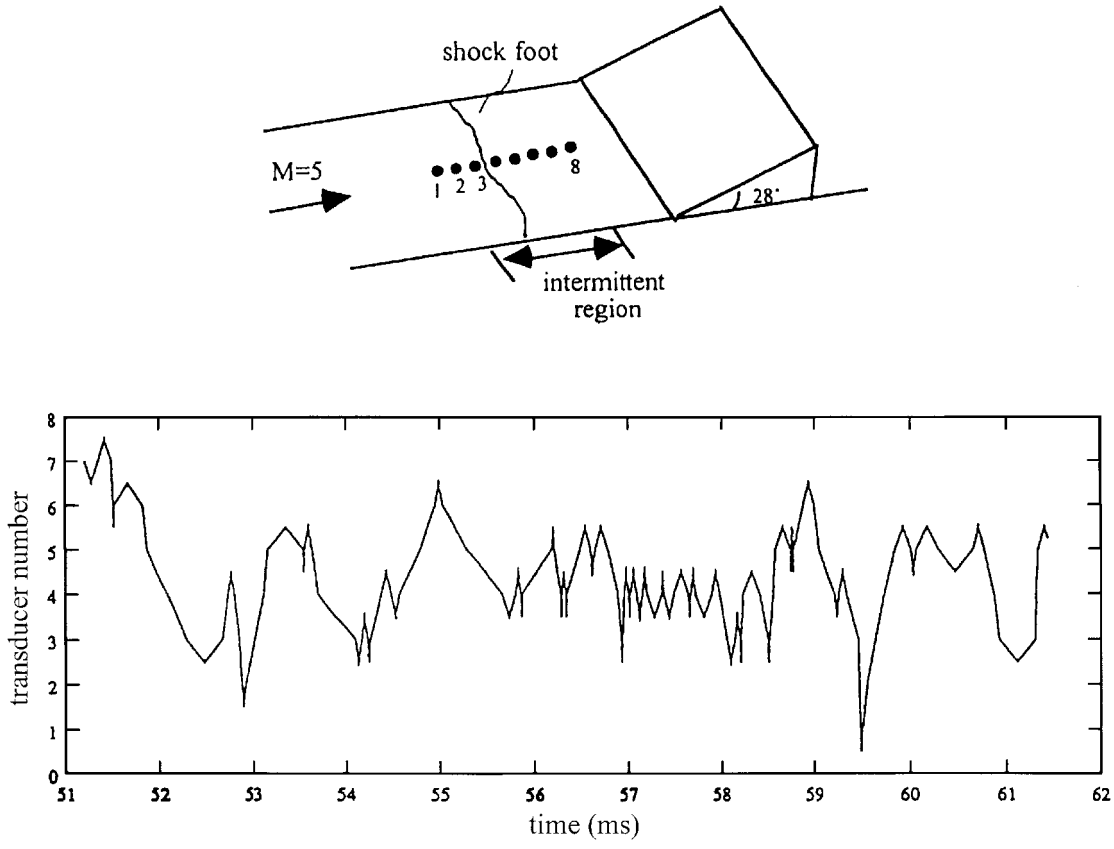

Fig. 1 Sample history of the shock foot position in an interaction generated by an unswept compression ramp (from Ref. 11).

PIV measurements of the turbulent velocity fluctuations in the incoming boundary layer were obtained and correlated with simultaneous measurements of the shock foot velocity. Previous work had suggested that a relationship between these two quantities might exist,[12] an idea supported by the large eddy simulations of Hunt and Nixon[18] that showed an approximately one-to-one relationship between the shock velocity and the incoming turbulent velocity fluctuations. However, the PIV measurements exhibited no such trend.

In the present study, a large-volume, high-accuracy PIV data set was acquired in the boundary layer upstream of a Mach 5 compression ramp interaction simultaneous with fast-response wall pressure measurements underneath the region of separation shock motion to determine the instantaneous shock foot position at the time of each PIV image. These data enabled an investigation of the relationship between the velocity fluctuations in the upstream boundary layer and the resulting shock foot motion. This was accomplished by computing ensemble averages of the velocity data conditioned on the behavior of the separation shock foot from which any subtle yet statistically significant correlations could be discerned. Such an approach was intended to reconcile some of the apparent inconsistencies in previous results and to enable a direct examination of the role of the upstream turbulent boundary-layer velocity fluctuations in the separation shock foot unsteadiness.

II. Experimental Program

A. Experimental Facility

All experiments were performed in the Mach 5 blowdown wind tunnel at the University of Texas at Austin. The test section had a constant cross-sectional area of 17.8×15.2 cm^2 (7×6 in.^{2}), and at the nozzle exit, the freestream Mach number was 4.95. The freestream unit Reynolds number was 49.5×10^6 m^{-1} (15.1×10^6 ft^{-1}) resulting from typical operating conditions of $P_0 = 2.31$ MPa (335 psia) and $T_0 = 356$ K (640°R). After transitioning naturally, the incoming boundary layer in the test section was fully turbulent and developed under nearly adiabatic wall temperature flow conditions.[14,19] The freestream velocity was found to be 750 m/s (2460 ft/s) (Ref. 20). The separated flowfield was generated by an unswept, full-span, 28-deg compression ramp, which previous studies have shown provides an unsteady separated flow whose streamwise length varies from about $2\delta_0$ to $4\delta_0$.

A fused silica window was installed in one side wall of the test section to provide optical access for the camera. The laser sheet passed through a narrow acrylic window in the ceiling of the test section and exited through a similar acrylic window in the test section floor. The latter window greatly reduced reflections from the tunnel floor, thus permitting measurements to be made closer to the wall.

B. Fluctuating Pressure Measurements

Multichannel fluctuating pressure measurements were made in the shock foot intermittent region, that is, the region of separation shock foot motion, to provide an indicator of the instantaneous shock foot location. The pressure measurements were made using fast-response transducers (Kulite Model XCQ-062-50A) flush-mounted in a plug inserted into the floor of the test section. The output from each transducer was low-pass filtered at 50 kHz and digitized to 12 bits at 100 kHz.

Two different transducer arrangements were used, as shown in Fig. 2, each incorporating five transducers. In the standard configuration, all five transducers were aligned in the streamwise direction with a center-to-center spacing of 2.92 mm (0.115 in.). The staggered arrangement consisted of one row of two transducers adjacent to a row of three transducers. In the latter case, the two rows were staggered in the streamwise direction by one-half of a transducer spacing, providing an effective streamwise transducer spacing of 1.46 mm (0.058 in.) and, thus, approximately doubling the spatial resolution. Neither arrangement fully spans the intermittent region, and so the compression ramp was moved relative to the pressure transducers to allow measurements to be made at different locations within the intermittent region.

The staggered transducer arrangement requires the assumption that the shock structure is essentially two dimensional, allowing measurements from the two-transducer row to be "inserted" into the gaps between the transducers of the three-transducer row. Support

for this supposition comes from wall pressure measurements made by Marshall and Dolling,[10] who used a full-span unswept compression ramp in the same facility. Their results showed that spanwise ripples in the shock foot typically have a streamwise amplitude less than $0.17\delta_0$ and a spanwise wavelength larger than $1.16\delta_0$. Thus, from one transducer row to the next (2.64 mm, or about $0.12\delta_0$), the shock foot can be considered essentially two dimensional.

The shock foot location was deduced from the fluctuating pressure signals using a modified form of the algorithms developed by Dolling and Brusniak[3] and Gramann and Dolling.[5] A two-threshold method converts each channel of pressure data to a binary signal denoting times when the shock is upstream of the transducer and when it is downstream. The resulting signals are nested together to bracket the instantaneous shock foot location between adjacent transducers, from which a trace of its position history is derived.

C. Particle Image Velocimetry

The PIV image acquisition system, shown in Fig. 3, used a dual-cavity Nd:YAG laser (Spectra Physics Quanta-Ray PIV-400) as the light source. The beams were frequency doubled to 532 nm and operated at 10 Hz, with the time between laser pulses ranging from 1.2 to 4.2 μs (accurate to within 0.2%). The scattered laser light was collected using a cross-correlation 1000×1000 pixel charge-coupled device camera (Kodak MegaPlus ES 1.0) digitized to 8 bits, in which each particle exposure is stored in a separate frame. The ES 1.0 camera has a maximum framing rate of 15 image pairs per second, but limitations in the software (SpeedVision OmniSpeed) reduced this to about 1.8 image pairs per second. However, the framing rate was doubled by using two identical cameras that imaged the same field of view through a cubic beam splitter. Four digital delay generators (Stanford Research Systems DG-535) were used to set the timing for the laser and cameras, which ensured that the second camera always captured a different pair of laser pulses than those captured by the first camera. Pressure data were acquired simultaneously using the pretriggering function of the analog-to-digital converter to provide data for about 20 ms both before and after image acquisition. During a typical test, 60 image pairs were obtained from each camera at an imaging location upstream of the farthest excursion of the separation shock, as shown in Fig. 2. Analysis of the image data was performed using PIV software developed in-house.[20] This software included optimization of window offsets between exposures for cross correlations and optional particle tracking to improve spatial resolution.

The particles used were aluminum oxide with a manufacturer's specification of 0.3-μm diam. An examination of particles from the seeder exit using a scanning electron microscope indicated that agglomeration resulted in a mean particle size closer to 1.0 μm, which is consistent with the observations of other researchers.[21,22] The Stokes number (the ratio of particle time response to the characteristic flow timescale) was estimated as about 0.8; therefore, the particles are expected to track the velocity fluctuations to within about 1% (Ref. 23). The particles were delivered using a two-stage seeder; the first stage was a dual fluidized bed, where two cylinders operated in parallel to entrain the particles in the airflow. Both fluidized beds fed tangentially into a cyclone separator that extracted only the smallest particles for seeding. A streamlined local injector delivered the particles into the flow at the exit plane of the wind-tunnel nozzle. This approach to seeding the flow was found to be necessary to produce adequate seeding densities, whereas previous

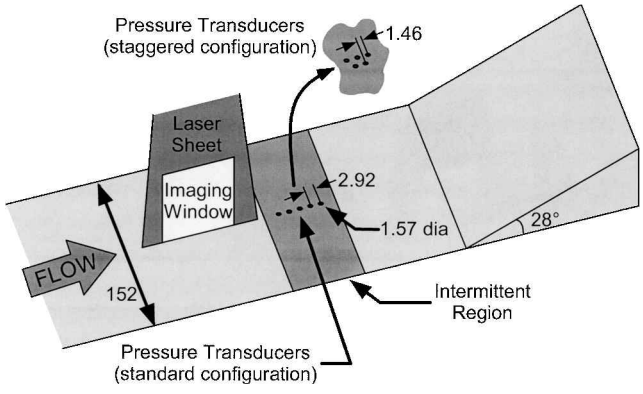

Fig. 2 Pressure transducer configurations for determining the separation shock foot motion, showing both the standard configuration and the staggered configuration as well as the location of PIV imaging window; dimensions in millimeters, not to scale.

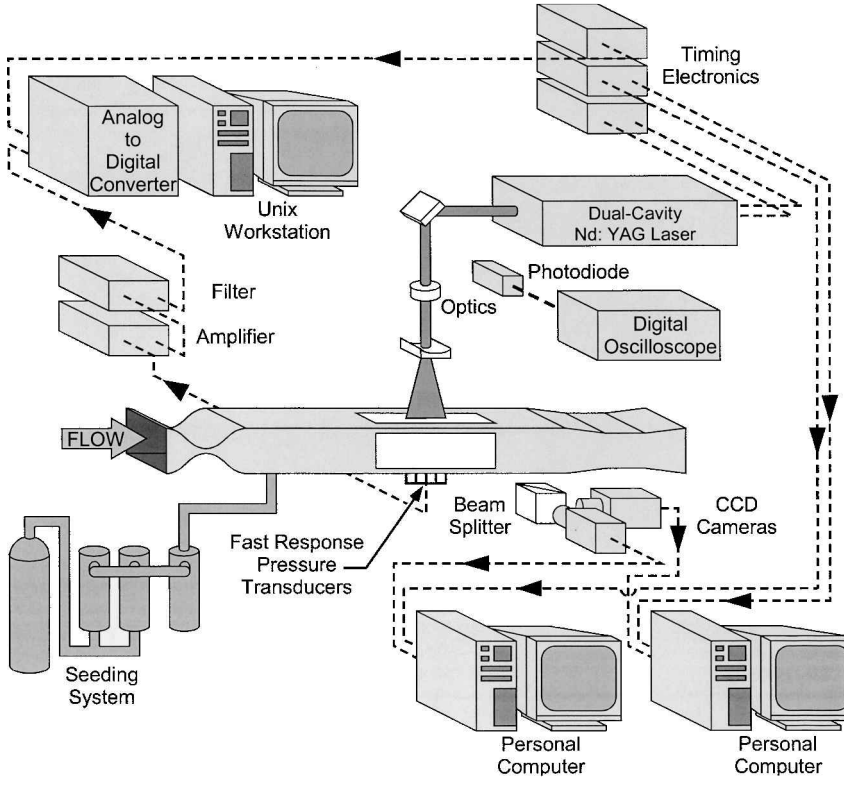

Fig. 3 Schematic diagram of the experimental system.

efforts involving seeding in the plenum were unsuccessful primarily because of the effects of the expansion of the flow through the nozzle and dispersion of the particles. The injector was 1.52 cm (0.6 in.) high, 1.40 cm (0.55 in.) wide, and 10.9 cm (4.3 in.) long; the leading- and trailing-edge surfaces were swept toward the center of the injector, yielding an appearance akin to a tapered diamond shape. It was located 78.7 cm (31 in.) upstream of the compression ramp corner, just upstream of the nozzle exit plane.

Because the injector was located at the nozzle exit rather than within the plenum, its influence on the test section flow required examination. Measurements showed that the injector thickened the boundary layer and perturbed its mean velocity profile, but wall pressure measurements indicated that, within the repeatability of the measurements, this had no significant effect on the separation shock foot dynamics. Such parameters as the shock foot intermittency, the mean pressure distribution, and the rms of the pressure fluctuations were essentially unchanged within the intermittent region. Furthermore, the power spectra of the pressure fluctuations beneath the incoming boundary layer maintained virtually the same shape with only a small difference in magnitude. These findings are consistent with earlier work using a pitot probe mounted upstream of the interaction in which it was found that the separation shock dynamics were essentially unchanged with the probe in place.[9,24,25]

D. Vector Processing

A large body of velocity data was acquired for both transducer arrangements at two different laser pulse separation times. In the standard case, about one-half of the image pairs were acquired with a pulse separation of 1.2 μs and the other half at 4.2 μs; the staggered configuration used pulse separations of 1.4 and 4.2 μs. The longer pulse separation time allowed the particles to undergo a substantially larger displacement and, hence, produced an improved dynamic range of the velocity measurements. However, it was subsequently discovered that the improved dynamic range was not nearly as helpful as the improved statistics associated with larger data sets. As such, no division in the data was made based on laser pulse separation, and only two distinct groups of data were produced, corresponding to the standard and the staggered transducer arrangements. For measurements concerned purely with shock location, the two configurations may be grouped together to produce one large data set. For those measurements concerning shock motion, these groups must necessarily remain separate because the measurements have different spatial resolutions and, therefore, are sensitive to different frequencies of motion. This yielded a data set of about 3240 image pairs each for the standard and staggered configurations.

The images were acquired with a field of view of approximately 30×30 mm^2 located within the incoming boundary layer with the downstream edge of the imaging window about 30 mm upstream of the separation shock's farthest excursion. The 1000×1000 pixel image pairs were processed using an interrogation window of 64×64 pixels and an overlap of about 50%, producing a 32×32 vector field with a resolution of about 2×2 mm^2 for each vector. The spanwise resolution was similar because the laser sheet was about 1.5 mm thick. Each interrogation window initially was processed using a streamwise offset between each exposure based on the mean boundary-layer velocity profile. The displacement resulting from this correlation was used to determine the proper offset for that specific vector and the correlation was recomputed using this offset. Use of an interrogation window offset optimized in this manner also optimizes the accuracy of the PIV velocity measurement, particularly for large velocity fluctuations near the wall.[26]

Standard validation of the vector field was performed based on the cross-correlation signal-to-noise ratio, but for this high-speed boundary-layer flow, a priori knowledge of the flowfield allowed for additional vector validation criteria. Given that the approximate turbulence levels are known for a boundary layer, this enabled limits to be placed on the range of magnitudes and angles that the vectors may have. Even with these more stringent validation criteria, the valid vector rate was in excess of 95 and 90% for the 1.2- and 4.2-μs laser pulse separation times, respectively.

Once vector fields were properly validated, they were collapsed into a mean velocity profile. The turbulent fluctuations for each individual vector field were found by subtracting from each vector the mean velocity information determined from the mean velocity profile for the corresponding experimental run. Variations in the profile from run to run were slight, but are significant when the velocity fluctuations are examined. The run-to-run variations resulted almost entirely from uncertainties in measuring the field of view of the camera and are less than 1% of U_∞. Because $\sqrt{u'^2}$ in the outer portion of the boundary layer is about 3% of U_∞, the relative uncertainty in $\sqrt{u'^2}$ is much larger, about 33%. However, subtracting the mean velocity profile generated using only those images acquired with identical camera positions removes much of this variation because the same error is present in both the instantaneous and mean measurements. Thus, it is a removable bias and the uncertainty in $\sqrt{u'^2}$ associated with the camera position is reduced to about 1%. Other contributors, principally precision uncertainty, raise the total uncertainty in $\sqrt{u'^2}$, and therefore, specific uncertainty estimates are provided with each velocity profile to be shown.

III. Results

A. Correlation of Upstream Boundary-Layer Properties with Shock Position

Prior studies suggested that a relationship exists between the thickness and/or shape of the upstream boundary layer and the separation shock foot position. To test these hypotheses, the PIV data were analyzed by sorting the vector fields into groups defined by the location of the shock foot at the time the flow in the particular PIV imaging window convected through the intermittent region. The position of the separation shock foot can be described using the shock foot intermittency γ, which denotes the percentage of time the shock foot spends upstream of the measurement station. Vector fields were placed into shock-upstream and shock-downstream groups corresponding to times at which the shock was upstream of the $\gamma = 20\%$ station or downstream of the $\gamma = 80\%$ station, respectively. Because the imaged region was upstream of the interaction, a finite convection time was required for the flow to reach the intermittent region. To account for the delay for the flow in the field of view to reach the center of the intermittent region, the pressure data were temporally shifted by a time corresponding to a convection velocity of $0.9U_\infty$ (Ref. 19). The results to be discussed were found to be insensitive to small variations in this time delay.

It was required that the shock remained within the upstream or downstream region for at least 100 μs to exclude those events during which the shock foot only briefly crossed a pressure transducer before altering direction and returning toward the center of the intermittent region. Vector fields within each of these two groups were then ensemble averaged and collapsed into the conditional mean velocity profiles shown in Fig. 4. The unconditional mean velocity profile compiled from all 6480 vector fields lies between the two conditional profiles, but for clarity is not shown.

The uncertainty estimates in Fig. 4 were determined by examining the unconditional velocity profiles computed for numerous individual experimental runs and quantifying their deviation from the mean velocity profile. A conservative estimate of the uncertainty was derived from this analysis and is shown in Fig. 4 as 95% confidence intervals. Much of the variation likely results from the small uncertainty in the camera position, as described in Sec. II.D. The details of this uncertainty analysis are provided in Ref. 20.

The atypical shape of the velocity profiles in Fig. 4 is the result of the particle injector's effect on the boundary layer, which adds a wakelike component to the velocity profile. The fact that the velocity does not asymptotically approach the freestream value does not indicate that the boundary-layer edge is outside the field of view, but rather indicates that the data suffer from a seeding bias caused by the addition of particles into the boundary layer but not the freestream. Because of the lack of seed particles in the freestream, regions that contain a large amount of freestream fluid will not be adequately sampled. This creates a bias toward boundary-layer velocities at the expense of freestream velocities and explains why the velocity profile fails to reach a constant freestream value.

Because the seeding bias is unrelated to the shock motion, it is present in both unconditional and conditional profiles and is, therefore, not responsible for any differences between them. The bias

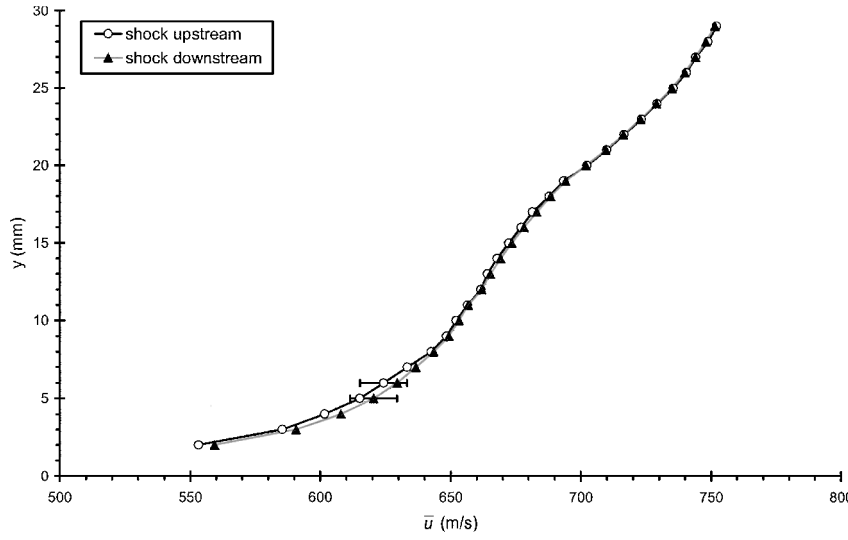

Fig. 4 Conditional ensemble average velocity profiles in the incoming boundary layer for shock-upstream and shock-downstream cases.

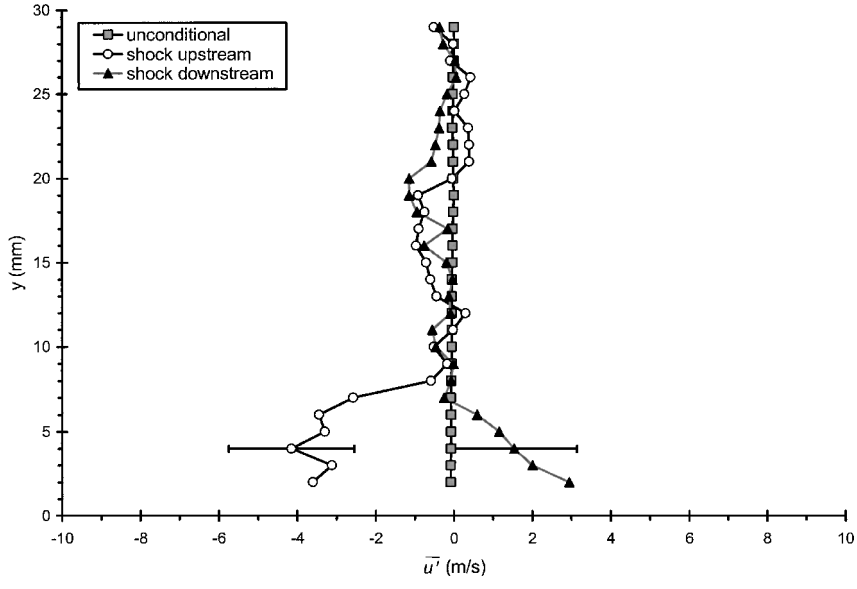

Fig. 5 Conditional ensemble average profiles of the streamwise velocity fluctuations in the incoming boundary layer for shock-upstream, shock-downstream, and unconditional cases.

influences which velocities can be measured, but unless the conditional sampling analysis already exhibits a preference for some particular range of velocities, the bias will not affect the conditional profiles differently than the unconditional profiles. Hence, whereas the seeding bias conceivably could influence the strength of a correlation based on the shock foot behavior if it is associated with high velocity fluid, it cannot manufacture a correlation where one does not already exist. Furthermore, even a bias in the magnitude is unlikely because, as will be shown later, correlations were found only in the lower portion of the boundary layer, below the region where the bias in the intermittent portion of the boundary layer could become a factor.

A close examination of the two profiles in Fig. 4 indicates that, despite the seeding bias near the freestream, no significant variation in boundary-layer thickness occurs with shock position. The similarity in the outer velocity profile between the shock-upstream and shock-downstream conditions is consistent with previous PLS studies,[15–17,27] as well as preliminary PIV measurements that employed different conditional analysis techniques.[16] Overall, these observations suggest that a low-frequency thickening/thinning of the upstream boundary layer[9,14] does not drive the large-scale separation shock motion.

Whereas no difference between the conditional mean velocity profiles is evident in the outer boundary layer, nearer to the wall the profile is slightly fuller for the shock-downstream case than for the shock-upstream case. Although this difference is very small, it appears to be physically real because varying parameters such as the size of the initial data set and the residency time required of the shock foot still yields a consistently similar difference between the two conditional profiles. Furthermore, this observation agrees with the earlier exploratory work of Beresh et al.[16] However, to substantiate this difference in the velocity profile shape, the measurement uncertainty must be reduced.

As described in Sec. II.D, an examination of the mean velocity fluctuation data, as opposed to the mean velocities themselves, has the benefit of removing the bias due to the uncertainty in camera position. Figure 5 shows conditional mean profiles analogous to those of Fig. 4, except here they are compiled from u' data. The unconditional profile also is shown and, as expected, is everywhere almost perfectly zero. The conditional profiles do exhibit a difference and show that when the shock is located upstream, the velocity fluctuations in the upstream boundary layer tend to be negative, and when it is located downstream, the velocity fluctuations tend to be positive. Furthermore, this difference is seen only in the lower part

of the boundary layer. Figure 5 shows that the subtle difference in the conditional profile shape seen in Fig. 4 is indeed real. However, it is quite small; although the difference in the velocity fluctuation magnitude is greater than the uncertainty estimates, it is less than 10 m/s or about 1% of U_∞.

B. Correlation of Velocity Fluctuations with Shock Motion

Because the present data set is an order of magnitude larger than that of the initial investigation,[17] it offered an opportunity to reexamine the idea that upstream turbulent velocity fluctuations correlate with the shock velocity. Mean velocity fluctuations in the upstream boundary layer were plotted against the shock velocity as determined from the rate of change of shock foot position. No distinguishable trend was found, even for repeated analyses employing only those vectors close to the wall or using the improved resolution of the shock velocity made possible by the staggered transducer configuration. In the interest of brevity, the associated figures are not presented in this paper; details may be found elsewhere.[20,28]

The lack of any such trend is, at first glance, contrary to Hunt and Nixon's[18] very large eddy simulation work. This may, however, be attributable to limitations on the frequencies of shock foot motion that are measurable in the present experiment. The highest resolvable shock frequency is about 4 kHz with the standard transducer configuration and somewhat higher with the staggered configuration, but the frequency of the boundary-layer velocity fluctuations associated with large-scale turbulent structures is approximately an order of magnitude larger. The values of u' may contain a component on the order of 4 kHz that is simply obscured by the higher-frequency fluctuations and, thus, leads to the lack of correlations. If it were possible to measure the shock velocity at frequencies of about 40 kHz to match the large-scale boundary layer turbulence, a correlation might emerge.

Because the shock velocity cannot be ascertained to arbitrarily high frequencies, a better method for examining a possible relationship between the boundary-layer velocity fluctuations and the shock motion is to use ensemble averages, similar to those computed for the shock foot position in Sec. III.A. Conditional velocity fluctuation profiles were again calculated, but in this case they were based on the motion of the separation shock foot rather than its position. Because the shock foot motion is defined as the distance it travels in a specified time period, it is quantified somewhat differently for the staggered and standard transducer arrangements, and therefore, data for each configuration were analyzed separately. Conditional profiles were characterized by the number of transducers the shock crosses without altering its direction in a specified time period. As in the earlier shock position analysis, a time delay based on $0.9U_\infty$ was incorporated into the triggering algorithm to account for the convection of the flow in the imaging window into the shock foot intermittent region. The actual times of the transducer crossings are irrelevant to the analysis so long as they occur within the specified time period. Shock motions not observed to be unidirectional were discarded because they may have been influenced by more than one type of boundary-layer velocity fluctuation.

Conditional mean profiles of the velocity fluctuations were acquired for both transducer arrangements for time periods of 100 (10), 250 (4), and 500 μs (2 kHz). Seven different conditions were used: upstream motions of one transducer spacing ($0.125\delta_0$ for the standard transducer configuration and $0.062\delta_0$ for the staggered configuration), two transducer spacings ($0.250\delta_0$ standard and $0.125\delta_0$ staggered), and three transducer spacings ($0.375\delta_0$ standard and $0.187\delta_0$ staggered); downstream motions of one, two, and three transducer spacings; and no motion at all. The resulting velocity profiles are shown in Figs. 6 and 7 for the standard and staggered transducer configurations, respectively. Within the 100-μs window, motions of three transducer spacings were too few to be statistically useful and are omitted. Uncertainty estimates again were conservatively estimated from an analysis of the variations observed between multiple unconditional mean profiles.

From Figs. 6 and 7, it is evident that little difference exists in the outer region of the boundary layer for the different shock motion conditions. Near the wall, however, a systematic variation in the velocity fluctuations can be seen. The trend is most evident for the standard transducer configuration in the 250-μs window as seen in Fig. 6b. Shocks that do not move within this time period are, on average, correlated with zero velocity fluctuation from the mean. Shocks that move upstream correlate with negative velocity fluctuations, the magnitude of which is dependent on the distance the shock has traversed. Similarly, shocks that move downstream correlate with positive velocity fluctuations whose magnitude is dependent on the distance the shock has moved. Furthermore, this relationship is strongest closer to the wall; with increasing distance from the wall, the correlation weakens until no difference exists between the seven conditions. This correlation of negative velocity fluctuations with upstream shock motions and vice versa is precisely that shown by the simulations of Hunt and Nixon,[18] although the magnitude of the fluctuations found here is significantly lower. Because Hunt and Nixon did not comment on a vertical dependence, it is not known if the simulations show the same result.

The same trend also can be seen for the 100-μs window, where the correlation is clear for motions of one transducer spacing but less apparent for longer motions. The latter is a result of the small number of events for these longer motions, but the profiles appear to follow the same trend. Though not shown here, a similar analysis utilizing a 50-μs window provides statistically useful profiles only for one-transducer shock motions, but these, too, follow the observed trend.[20] On the other hand, lengthening the time window to 500 μs, as shown in Fig. 6c, diminishes the correlation. It appears, then, that a time window longer than 100 μs is required to detect a sufficient number of samples of longer shock motions, but the greater duration of the 500-μs window allows the inclusion of multiple events that mask the influence of the velocity fluctuations on the shock foot motion. Thus, limitations in the present experimental methodology for tracking the shock foot motion may restrict the detection of a correlation to only simple shock foot events. If a correlation does indeed exist at lower frequencies (longer time windows), it may become more subtle and require larger ensemble averages to remove the effects of the higher frequency fluctuations.

The same correlation between upstream velocity fluctuations and the shock foot motion also was seen using the staggered transducer configuration in Fig. 7. The trend is most evident for the 100-μs time window in Fig. 7a. No profiles are shown for three-transducer motions due to statistically inadequate ensemble averages. For the 250-μs window of Fig. 7b, however, the trend has begun to fade. Upstream shock motions still correlate with negative velocity fluctuations, though the two- and three-transducer motions have exchanged positions, but the profiles for downstream shock motions are not meaningfully distinguishable from zero. Once the triggering window has been expanded to 500 μs in Fig. 7c, no correlation is evident.

In general, the profiles for the staggered configuration exhibit more noise than those for the standard configuration. This is probably because the number of events corresponding to a unidirectional shock motion is reduced by nearly half because five staggered transducers do not cover as large a fraction of the intermittent region as five nonstaggered transducers. Thus, it is more likely that at any given time the shock foot is not located in an instrumented region. Despite fewer events, however, essentially the same relationship between velocity fluctuations and the shock foot motion can be seen in Fig. 7 as in Fig. 6. In particular, the time window at which the trend appears strongest has shifted to 100 μs for the staggered transducer configuration from 250 μs for the standard configuration, suggesting that the smaller transducer spacing allows measurement of a correlation at higher frequencies. Like the standard configuration, the disappearance of the correlation at low frequencies cannot simply be attributed to inadequate statistics because the precision uncertainty is relatively low in Fig. 7c.

Although a correlation is evident between the turbulent velocity fluctuations in the incoming boundary layer and the motion of the separation shock foot, the difference between the unconditional profile and the conditional profiles is only about 1–3% of the freestream velocity. The conditional mean velocity fluctuations of 10–20 m/s in magnitude (Fig. 6) appear low when compared with values of 50–80 m/s for $\sqrt{u'^2}$ found near the wall. However, the 10–20-m/s value is physically consistent. A shock motion of two transducer

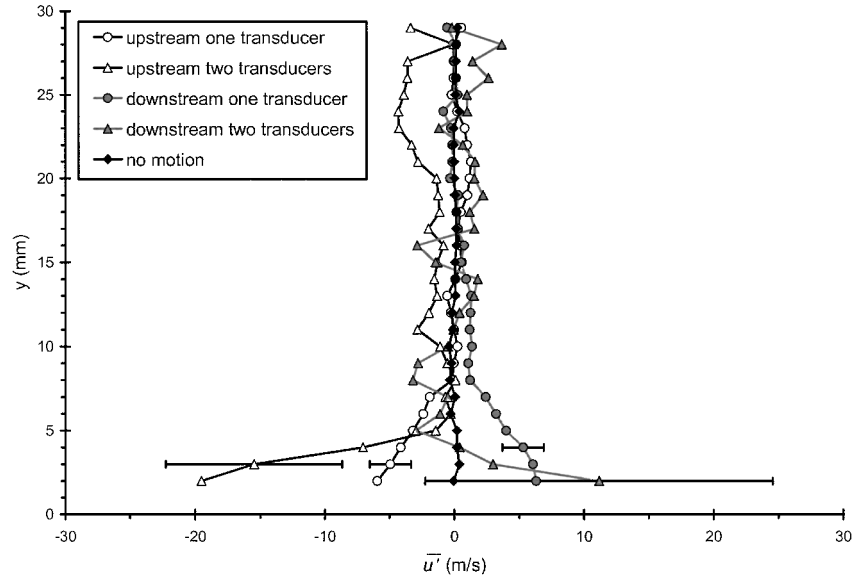

a)

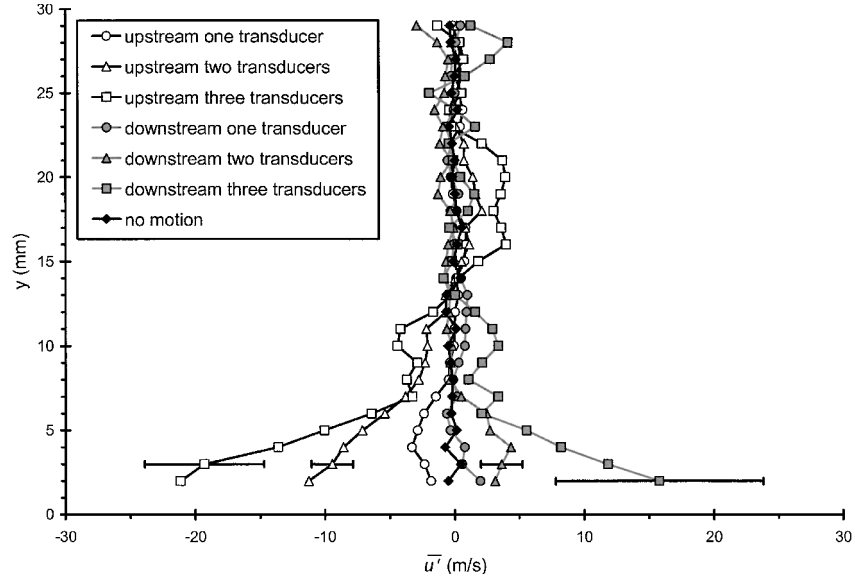

b)

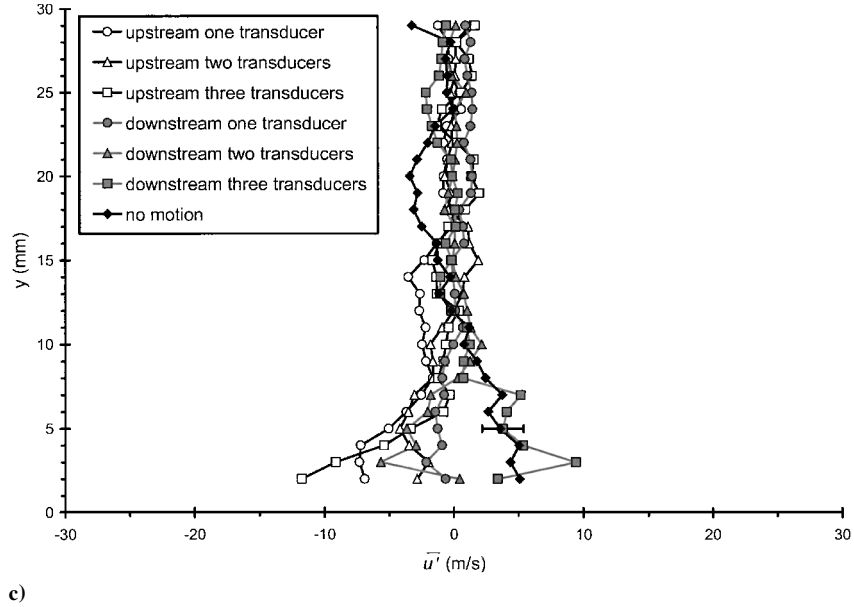

c)

Fig. 6 Conditional ensemble average profiles of the streamwise velocity fluctuations in the incoming boundary layer conditioned on the separation shock foot motion within a time period of a) 100, b) 250, and c) 500 μs. Measurements were made using the standard pressure transducer configuration.

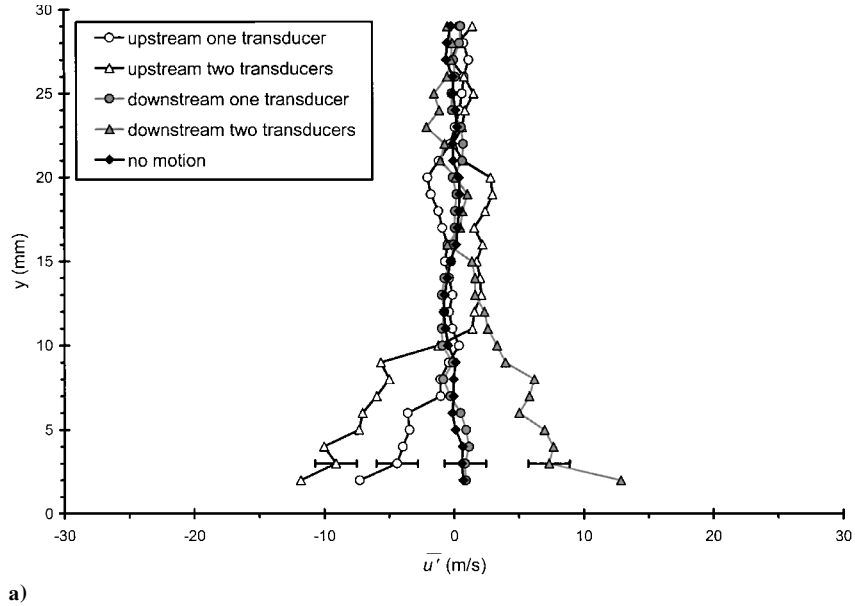

a)

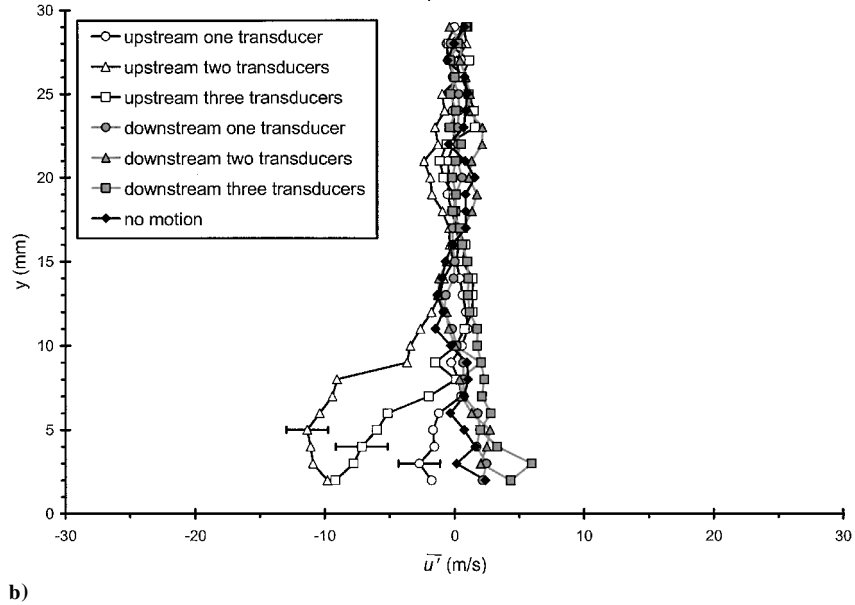

b)

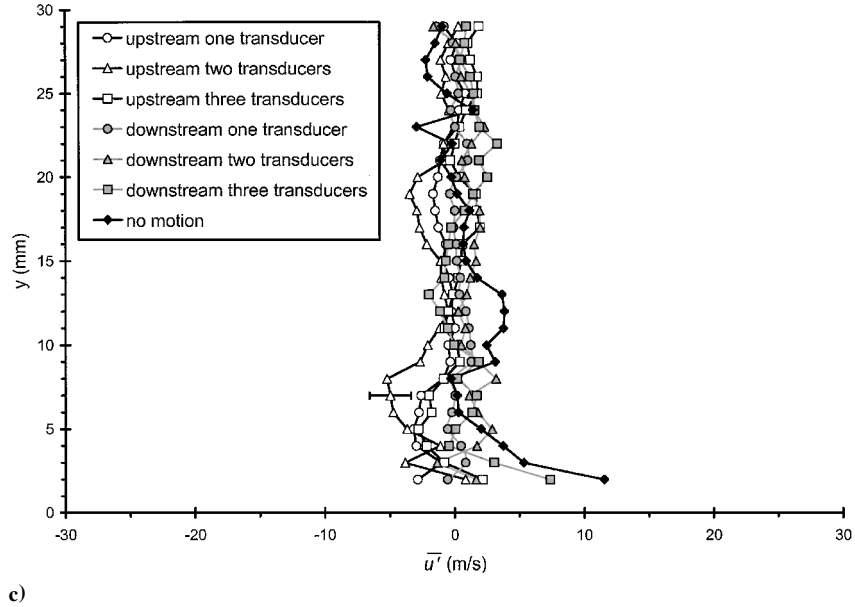

c)

Fig. 7 Conditional ensemble average profiles of the streamwise velocity fluctuations in the incoming boundary layer conditioned on the separation shock foot motion within a time period of a) 100, b) 250, and c) 500 μs. Measurements were made using the staggered pressure transducer configuration.

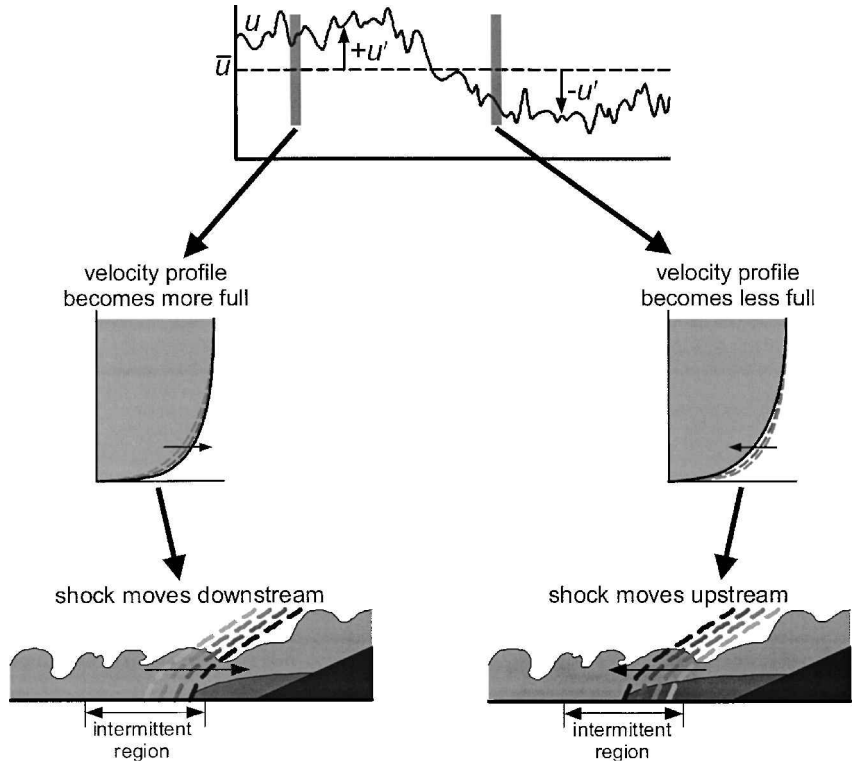

Fig. 8 Relationship between the incoming turbulent boundary layer and the separation shock foot unsteadiness.

spacings means that the shock must move 5.8 mm (for the standard configuration) in the time window. For a 250-μs window, this corresponds to a shock velocity of 23 m/s, which is of the same order of magnitude as the upstream velocity fluctuations.

The correlation between the velocity fluctuations and the shock foot motion actually may be stronger than presented because of limitations in the ability of the present experimental apparatus to resolve the shock position. Because the shock foot motion serves as the trigger mechanism for event detection, any uncertainties in detecting the shock position may introduce data into the ensemble averages that do not actually belong, thus obscuring the correlation. Spatial limitations due to the physical size of the pressure transducers are the most fundamental obstacle. Passage of the shock foot is known only at five locations in the intermittent region, leading to a relatively low-resolution estimate of the shock foot position, even for the staggered configuration. Further uncertainties may arise from the assumption of a single sharp shock front, when in fact the shock structure near the wall may be more complicated.[6,27]

IV. Discussion of Results

A simple physical explanation for the effects of the upstream boundary layer on the separation shock unsteadiness can be deduced from the preceding observations and is illustrated in Fig. 8. The data suggest that, when positive velocity fluctuations occur in the incoming boundary layer, the velocity profile is momentarily fuller, which imparts an increased resistance to separation that yields a downstream motion of the separation shock. Analogously, negative velocity fluctuations result in upstream shock motion as the interaction responds to the less-full shape of the velocity profile. Continuous variations in the upstream velocity fluctuations induce the unsteady shock foot motion.

Despite the clear correlations seen in Figs. 6 and 7, it is possible that the relationship between the velocity fluctuations and shock motion does not represent the fundamental relationship that drives the interaction unsteadiness. It can be argued that the shock fundamentally responds to the rate of change in the shape of the upstream velocity profile rather than to fluctuations with respect to the mean velocity. For example, the proposed model implies that a shock moving downstream corresponds to an upstream velocity profile that has become fuller than it was previously. Although this is a positive acceleration, it could be a negative velocity fluctuation, that is, lower than the mean velocity, provided it was "less negative" than the velocity fluctuation a short time before. As another example, a positive velocity fluctuation that remains constant for a relatively long period of time obviously would exhibit no change in the velocity profile. Despite that a positive velocity fluctuation occurs, the profile would maintain the same resistance to separation, and no motion of the shock would be expected. Such examples imply that a stronger correlation would be found between the shock foot motion and the upstream boundary-layer acceleration (or more precisely, the time rate of change of the velocity profile shape), rather than with the velocity fluctuations. Additional experiments are required to examine this idea further.

It is probable that the correlation of the velocity profile shape with shock position, as shown in Fig. 5, is an artifact of a more fundamental correlation between the velocity profile and the shock motion. Changes in the shape of the velocity profile can induce motion of the shock foot, but the probability of a motion occurring is dependent on the starting location of the separation shock. The shock cannot move arbitrarily far upstream or downstream, so that if the shock is in an upstream location a positive velocity fluctuation is likely to cause a downstream shock motion. However, a negative velocity fluctuation would attempt to move the shock upstream, but if it is already in an extreme upstream location, it is unlikely to move substantially farther. Under this scenario, an ensemble average based on an upstream shock location will be biased toward those fluctuations that tend to keep the shock upstream, that is, negative fluctuations, which make the profile "less full." A similar argument can be made for shocks initially at the downstream end of the intermittent region. The present results seem to support this idea because the magnitude of the ensemble average velocity fluctuations that correlate with the shock motion are generally about 10 m/s and as high as 20 m/s (Fig. 6), whereas the difference between the conditional mean velocity profiles with the shock foot at extreme upstream and downstream locations is only about 6 m/s (Fig. 5).

Another interesting result of this analysis concerns the frequencies of the separation shock motion. Previous studies have noted an apparent fundamental mismatch between the characteristic turbulent frequencies in the upstream boundary layer, which in this case occur at about 40 kHz for large-scale structures, and the shock foot

motion, at about 0.1–4 kHz (Refs. 8, 12, 18, and 25). To explain this, it has been proposed that two coexisting mechanisms exist, one a high-frequency source driving the small-scale shock motion and the other a low-frequency source driving the large-scale shock motion. However, it is well known that the power spectrum of turbulent velocity fluctuations is broadband; that is, it spans a continuous range of frequencies from essentially dc to those that characterize the dissipation scale. It may be that the shock responds to this broad range of frequencies, but motion has been detected just at low frequencies because only the low-frequency fluctuations can cause large-scale movement discernable by the spatial resolution of the pressure transducers. In other words, the shock may exhibit unsteadiness at a wide range of frequencies, but the motion detection system (transducer arrays) filters out the effect of the higher frequency forcing.

It is also possible, however, that the cause of the low-frequency fluctuations is some type of facility-dependent forcing, which has its origins in other than flat-plate boundary-layer turbulence. Ünalmis and Dolling's[24] data indicate that the tunnel floor boundary layer has an "underlying weak vortical structure" perhaps resulting from Görtler vortices generated during expansion through the nozzle. Such vortices may induce lower frequency velocity fluctuations into the flow that drive the shock motion at these frequencies simultaneously with the boundary-layer large-scale turbulence driving it at higher frequencies. However, because the low-frequency unsteadiness of shock-induced turbulent separation has been observed in a range of facilities operating at different Mach and Reynolds numbers, any nonturbulent source must be present in all of these facilities to the same degree, which seems unlikely. Nevertheless, the significance of the present work is in the identification of the relationship between the upstream velocity fluctuations and the shock foot motion, regardless of the source of those fluctuations.

Although much of this discussion is speculative and highlights the need for new experiments, the present results are consistent with earlier research. They are consistent with the large eddy simulations of Hunt and Nixon,[18] with Erengil and Dolling's[12] correlations between pressure fluctuations in the upstream boundary layer and the shock velocity, and Ünalmis and Dolling's[24] suggestion that Görtler vortices may play a role in the large-scale shock motion. Furthermore, it should be emphasized that the existence of a relationship between the upstream turbulent boundary layer velocity fluctuations and shock motion does not exclude the possibility of other influences on the shock motion. Most notably, a relationship may exist between the shock motion and fluctuations downstream of it, as has been postulated by Plotkin.[29]

V. Conclusions

To examine the relationship between incoming boundary-layer properties and the unsteadiness of a shock-induced separated flow, a large quantity of PIV data was obtained in the boundary layer just upstream of the interaction simultaneous with fluctuating wall pressure measurements beneath the unsteady separation shock foot. Ensemble average velocity profiles derived from the PIV data were computed conditioned on the instantaneous location of the separation shock foot within the intermittent region, as derived from the wall pressure measurements. Mean velocity profiles for shock-upstream and shock-downstream positions found no difference in the boundary-layer thickness with shock position, in agreement with previous planar laser imaging experiments. This suggests that a thickening/thinning boundary layer is probably not the cause of the shock unsteadiness, as was proposed in earlier work. Ensemble average velocity fluctuations conditioned on different types of separation shock foot motion showed that although no significant distinction was apparent in the outer region of the boundary layer, nearer to the wall, positive velocity fluctuations correlated with downstream shock motions and vice versa. Furthermore, larger fluctuations corresponded to longer shock excursions. These observations are consistent with the physical principle wherein a momentarily fuller velocity profile imparts greater resistance to separation to the boundary layer and, hence, induces a downstream shock motion and vice versa. These results are the first to offer direct experimental evidence of a relationship between the velocity fluctuations in the upstream boundary layer and the motion of the separation shock foot. This clearly represents a significant source of the unsteadiness of shock-induced turbulent separation; however, it is not known at this time if it the sole mechanism, or only one of several contributing mechanisms.

Acknowledgments

This research was supported through Grants DAAH04-94-G-0190, DAAG55-98-1-0290, and DAAG55-98-1-0062 from the Army Research Office monitored by T. Doligalski. The authors gratefully acknowledge this source of funding.

References

[1]Andreopoulos, J., and Muck, K. C., "Some New Aspects of the Shock-Wave/Boundary-Layer Interaction in Compression Ramp Flows," *Journal of Fluid Mechanics*, Vol. 180, 1987 pp. 405–428.

[2]Kussoy, M. I., Brown, J. D., Brown, J. L., Lockman, W. K., and Horstman, C. C., "Fluctuations and Massive Separation in Three-Dimensional Shock Wave/Boundary Layer Interactions," *Transport Phenomena in Turbulent Flows: Theory, Experiment, and Numerical Simulation; Proceedings of the Second International Symposium on Transport Phenomena in Turbulent Flows*, Tokyo, 1987, pp. 875–887.

[3]Dolling, D. S., and Brusniak, L., "Separation Shock Motion in Fin, Cylinder, and Compression Ramp Induced Turbulent Interactions," *AIAA Journal*, Vol. 27, No. 6, 1989, pp. 734–742.

[4]Gramann, R. A., and Dolling, D. S., "Dynamics of Separation and Reattachment in a Mach 5 Unswept Compression Ramp Flow," AIAA Paper 90-0380, Jan. 1990.

[5]Gramann, R. A., and Dolling, D. S., "Detection of Turbulent Boundary-Layer Separation Using Fluctuating Wall Pressure Signals," *AIAA Journal*, Vol. 28, No. 6, 1990, pp. 1052–1056.

[6]Erengil, M. E., and Dolling, D. S., "Unsteady Wave Structure Near Separation in a Mach 5 Compression Ramp Interaction," *AIAA Journal*, Vol. 29, No. 5, 1991, pp. 728–735.

[7]Selig, M. S., and Smits, A. J., "Effect of Periodic Blowing on Attached and Separated Supersonic Turbulent Boundary Layers," *AIAA Journal*, Vol. 29, No. 10, 1991, pp. 1651–1658.

[8]Erengil, M. E., and Dolling, D. S., "Correlation of Separation Shock Motion with Pressure Fluctuations in the Incoming Boundary Layer," *AIAA Journal*, Vol. 29, No. 11, 1991, pp. 1868–1877.

[9]McClure, W. B., "An Experimental Study of the Driving Mechanism and Control of the Unsteady Shock Induced Turbulent Separation in a Mach 5 Compression Corner Flow," Ph.D. Dissertation, Dept. of Aerospace Engineering and Engineering Mechanics, Univ. of Texas, Austin, TX, Aug. 1992.

[10]Marshall, T. A., and Dolling, D. S., "Computation of Turbulent, Separated, Unswept Compression Ramp Interactions," *AIAA Journal*, Vol. 30, No. 8, 1992, pp. 2056–2065.

[11]Dolling, D. S., "Fluctuating Loads in Shock Wave/Turbulent Boundary Layer Interaction: Tutorial and Update," AIAA Paper 93-0284, Jan. 1993.

[12]Erengil, M. E., and Dolling, D. S., "Physical Causes of Separation Shock Unsteadiness in Shock Wave/Turbulent Boundary Layer Interactions," AIAA Paper 93-3134, July 1993.

[13]Brusniak, L., and Dolling, D. S., "Physics of Unsteady Blunt-Fin-Induced Shock Wave/Turbulent Boundary Layer Interactions," *Journal of Fluid Mechanics*, Vol. 273, 1994, pp. 375–409.

[14]Ünalmis, O. H., and Dolling, D. S., "Decay of Wall Pressure Field and Structure of a Mach 5 Adiabatic Turbulent Boundary Layer," AIAA Paper 94-2363, June 1994.

[15]Chan, S. C., "Planar Laser Scattering Imaging of Shock Wave Turbulent Boundary Layer Interactions," M.S. Thesis, Dept. of Aerospace Engineering and Engineering Mechanics, Univ. of Texas, Austin, TX, Nov. 1996.

[16]Beresh, S. J., Clemens, N. T., Dolling, D. S., and Comninos, M., "Investigation of the Causes of Large-Scale Unsteadiness of Shock-Induced Separated Flow Using Planar Laser Imaging," AIAA Paper 97-0064, Jan. 1997.

[17]Beresh, S. J., Comninos, M., Clemens, N. T., and Dolling, D. S., "The Effects of the Incoming Turbulent Boundary Layer Structure on a Shock-Induced Separated Flow," AIAA Paper 98-0629, Jan. 1998.

[18]Hunt, D., and Nixon, D., "A Very Large-Eddy Simulation of an Unsteady Shock Wave/Turbulent Boundary Layer Interaction," AIAA Paper 95-2212, June 1995.

[19]Ünalmis, O. H., and Dolling, D. S., "Decay of Fluctuating Wall-Pressure Field of a Mach 5 Turbulent Boundary Layer," *AIAA Journal*, Vol. 37, No. 9, 1999, pp. 1088–1096.

[20]Beresh, S. J., "The Effect of the Incoming Turbulent Boundary Layer on a Shock-Induced Separated Flow Using Particle Image Velocimetry," Ph.D. Dissertation, Dept. of Aerospace Engineering and Engineering Mechanics, Univ. of Texas, Austin, TX, Aug. 1999.

[21]Urban, W. D., and Mungal, M. G., "Planar Velocity Measurements in Compressible Mixing Layers," *Journal of Fluid Mechanics*, Vol. 431, 2001, pp. 189–222.

[22]Humphreys, W. M., Jr., and Bartram, S. M., "Using Particle Image Velocimetry in Difficult Facilities: Some Lessons Learned," AIAA Paper 96-2267, June 1996.

[23]Samimy, M., and Lele, S. K., "Motion of Particles with Inertia in a Compressible Free Shear Layer," *Physics of Fluids A*, Vol. 3, No. 8, 1991, pp. 1915–1923.

[24]Ünalmis, O. H., and Dolling, D. S., "Experimental Study of Causes of Unsteadiness of Shock-Induced Turbulent Separation," *AIAA Journal*, Vol. 36, No. 3, 1998, pp. 371–378.

[25]Gramann, R. A., and Dolling, D. S., "A Preliminary Study of Turbulent Structures Associated with Unsteady Separation Shock Motion in a Mach 5 Compression Ramp Interaction," AIAA Paper 92-0744, Jan. 1992.

[26]Westerweel, J., Dabiri, D., and Gharib, M., "The Effect of a Discrete Window Offset on the Accuracy of Cross-Correlation Analysis of Digital PIV Recordings," *Experiments in Fluids*, Vol. 23, No. 1, 1997, pp. 20–28.

[27]Comninos, M., "Investigation into the Cause of Unsteadiness of Shock Wave/Turbulent Boundary Layer Interaction using Planar Laser Scattering," M.S. Thesis, Dept. of Aerospace Engineering and Engineering Mechanics, Univ. of Texas, Austin, TX, Dec. 1997.

[28]Beresh, S. J., Clemens, N. T., and Dolling, D. S., "The Relationship Between Upstream Turbulent Boundary Layer Velocity Fluctuations and Separation Shock Unsteadiness," AIAA Paper 99-0295, Jan. 1999.

[29]Plotkin, K. J., "Shock Wave Oscillation Driven by Turbulent Boundary Layer Fluctuations," *AIAA Journal*, Vol. 13, No. 8, 1975, pp. 1036–1040.

R. M. C. So
Associate Editor